ELSEVIER

Journal of Physics and Chemistry of Solids 64 (2003) 2525–2533

JOURNAL OF PHYSICS AND CHEMISTRY OF SOLIDS

www.elsevier.com/locate/jpcs

Magnetic characterization of orthorhombic $LiMnO_2$ and electrochemically transformed spinel Li_xMnO_2 ($x < 1$)

Young-Il Jang[1], F.C. Chou, Biying Huang[2], Donald R. Sadoway, Yet-Ming Chiang*

Department of Materials Science and Engineering and Center for Materials Science and Engineering, Massachusetts Institute of Technology, Cambridge, MA 02139, USA

Received 28 May 2003; revised 14 August 2003; accepted 29 August 2003

Abstract

Orthorhombic $LiMnO_2$ exhibits complex magnetic behavior. In addition to short- and long-range antiferromagnetic ordering, we observed spin-glass behavior in the reported temperature regime of long-range antiferromagnetic ordering. Lithium extraction from $LiMnO_2$ further complicates its magnetic behavior. A broad maximum of susceptibility at $\approx$360 K, characteristic of well-ordered $LiMnO_2$, disappears upon electrochemical delithiation to $Li_{0.39}MnO_2$, indicating that two-dimensional ordering on the folded triangular Mn lattice in $LiMnO_2$ is destroyed as the cation sublattice begins to transform to a spinel. Spin-glass behavior is, however, observed in $Li_{0.39}MnO_2$ as well. Compared to conventionally prepared spinel $LiMn_2O_4$, a lower degree of frustration is deduced, which is attributed to incomplete spinel ordering in the early stages of the cycling-induced transformation. In addition, the fraction of Mn ions occupying tetrahedral sites during the spinel transformation has been quantitatively determined for the first time, using magnetic susceptibility data. The results, surprisingly, support the existence of low-spin Mn ions on tetrahedral sites in the electrochemically transformed spinel.

Keywords: D. Magnetic properties

1. Inroduction

Orthorhombic $LiMnO_2$ (space group *Pmnm*, hereafter referred to as *o*-$LiMnO_2$) and its doped counterparts are potential high-capacity cathode materials for rechargeable Li batteries [1–5]. In this compound, oxygen ions are arranged in nearly cubic-close-packing, and the octahedral interstices are occupied by Li and Mn forming corrugated (zig–zag) layers [2]. The neighboring MnO_6 octahedra share a common edge. Due to the presence of high-spin Mn^{3+} ($t_{2g}^3e_g^1$) on the octahedral sites, the local site symmetry around Mn^{3+} is distorted from a regular octahedron by a cooperative Jahn–Teller distortion. The Mn sublattice can be viewed as a folded triangular lattice, the fold angle being 111°. Each triangle is distorted to isosceles with one edge of 2.806 Å and the other two of 3.09 Å [6]. The ordered rocksalt structure of *o*-$LiMnO_2$ irreversibly transforms to a spinel-like cation ordering during electrochemical cycling [3–5,7–10].

Since magnetic properties depend critically on cation ordering, magnetic characterization can be used to probe the spinel transformation of *o*-$LiMnO_2$. To date the magnetic properties of an electrochemically transformed spinel have not been reported. In high temperature synthesized *o*-$LiMnO_2$, Greedan et al. [6] have reported that long-range antiferromagnetic ordering is established below 261 K with a magnetic structure having a propagation vector$k$ = (1/2 1/2 1/2). They proposed a collinear magnetic structure based on antiferromagnetic intrachain coupling along the *a*-axis and antiferromagnetic interchain coupling, considering that nearest neighbor Mn–Mn distance is shortest along the *a*-axis. Magnetic properties of well-ordered conventional spinel $Li_xMn_2O_4$ have also been studied previously

* Corresponding author. Tel.: +1-617-253-6471; fax: +1-617-253-6201.
E-mail address: ychiang@mit.edu (Y.-M. Chiang).
[1] Present address: Condensed Matter Sciences Division, Oak Ridge National Laboratory, Oak Ridge, TN 37831-6030, USA
[2] Present address: Valence Technology, Henderson, NV 89015

0022-3697/03/$ - see front matter © 2003 Elsevier Ltd. All rights reserved.
doi:10.1016/j.jpcs.2003.08.006

[11–27]. Both long-range antiferromagnetic ordering and spin-glass behavior have been observed in $Li_xMn_2O_4$ [13,20–23,25,26,28]. Since the transformed spinel is expected to be highly disordered in cationic configuration compared to conventional well-annealed spinel, especially during the initial lithiation and delithiation cycles, it may be possible to use magnetic characterization to understand structural differences between transformed spinel and highly-ordered, conventional spinel.

In this study, we characterized the magnetic properties of a starting well-ordered *o*-$LiMnO_2$ and a spinel $Li_{0.39}MnO_2$ that was transformed by electrochemical delithiation of the starting material. The effect of the spinel transformation on the magnetic properties has been investigated. We observe time- and frequency-dependent magnetization, indicative of spin-glass behavior in well-ordered *o*-$LiMnO_2$ that simultaneously exhibits the characteristics of long-range antiferromagnetic ordering. The magnetic properties of the transformed spinel are compared to those of *o*-$LiMnO_2$ and $Li_xMn_2O_4$ and interpreted in terms of cation ordering.

2. Experimental

o-$LiMnO_2$ was synthesized by firing finely divided freeze-dried Mn_3O_4 and LiOH precursors at $T = 850–950$ °C, $P_{O_2} = 10^{-6}$ atm for a total of 4–5 h. The oxide powder was furnace-cooled after the heat treatment. The oxide powders were then intermittently ground using an agate mortar and pestle at room temperature. The 950 °C-sample was ground once, and the 850 °C-sample twice. Details of the oxide powder cryosynthesis method are reported elsewhere [3,29–31]. Powders were characterized by X-ray diffraction (XRD) using Cu-K_α radiation at 60 kV, 300 mA (Rigaku RTP500RC). Electrochemical delithiation of *o*-$LiMnO_2$ was performed using a rechargeable Li cell with *o*-$LiMnO_2$ as the cathode. The weight percentage of the active material in the composite cathode was 69.8%. Details of the battery fabrication are described elsewhere [32]. *o*-$LiMnO_2$ was delithiated by charging the cell to 4.8 V at 24.6 mA/g rate. After the electrochemical treatment, the cell was disassembled and the cathode was dried and hermetically sealed in a glove box. Part of the cathode was separated for XRD analysis. Magnetic measurements were carried out in He atmosphere on the remaining cathode as well as on the as-synthesized *o*-$LiMnO_2$ compound, using a Quantum Design superconducting quantum interference device (SQUID) magnetometer.

3. Results and discussion

3.1. Starting *o*-$LiMnO_2$

Fig. 1 shows the powder XRD pattern of the starting *o*-$LiMnO_2$ after firing at $T = 950$ °C, $P_{O_2} = 10^{-6}$ atm for a total of 4 h. The *hkl* indices labeled in Fig. 1 are based on the space group *Pmnm*. The lattice parameters have been calculated from the XRD data by a least-squares method to be: $a = (2.8057 \pm 0.0003)$ Å, $b = (5.7490 \pm 0.0005)$ Å, and $c = (4.5754 \pm 0.0006)$ Å, in good agreement with the literature data [33]. It is notable that the full width at half maximum (fwhm) of the (011) peak at $2\theta = 24.8°$ is 0.13°. Croguennec et al. [34] correlated an increasing width of this peak with a higher density of monoclinic stacking faults occurring in *o*-$LiMnO_2$. The width of 0.13° in Fig. 1 corresponds to a negligible concentration of stacking faults (≈1%) according to their analysis, indicating that the starting material in this study has a well-ordered orthorhombic structure. No impurity phase was detected by XRD.

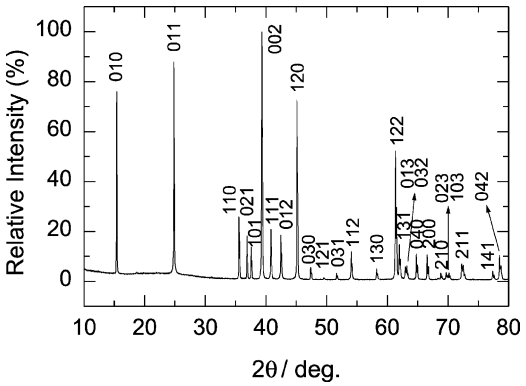

Fig. 1. X-ray diffraction pattern of *o*-$LiMnO_2$ after firing at $T = 950$ °C, $P_{O_2} = 10^{-6}$ atm for a total of 4 h. Miller indices *hkl* are indexed according to the *Pmnm* space group.

We measured the dc magnetization between 5 and 400 K in a magnetic field of 300 Oe after zero-field-cooling (ZFC) and field-cooling (FC), respectively, as shown in Fig. 2. The right inset shows a broad maximum centered at ≈360 K, consistent with the previous work on *o*-$LiMnO_2$ [6], which has been attributed to the onset of two-dimensional short-range spin correlations on the folded triangular lattice below

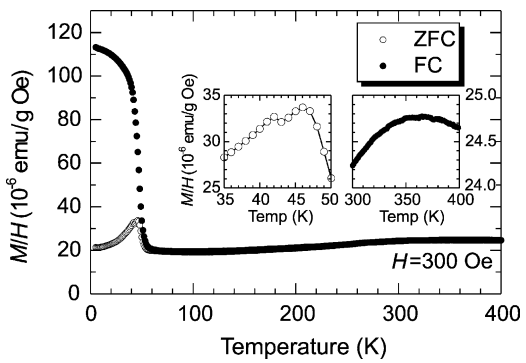

Fig. 2. Zero-field-cooled (ZFC) and field-cooled (FC) dc magnetization of *o*-$LiMnO_2$ as a function of temperature in a field of 300 Oe. The oxide sample was fired at $T = 950$ °C, $P_{O_2} = 10^{-6}$ atm for a total of 4 h.

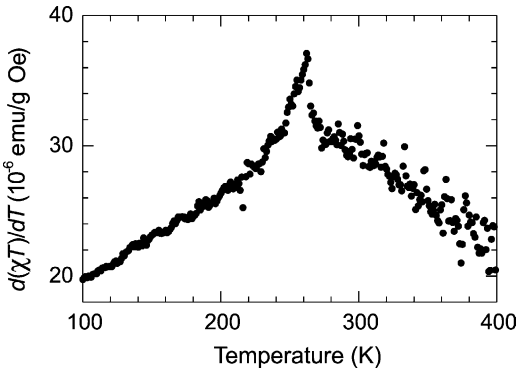

Fig. 3. d(χT)/dT versus T plot of o-$LiMnO_2$ identifying a transition at 262 K. The oxide sample was fired at $T = 950$ °C, $P_{O_2} = 10^{-6}$ atm for a total of 4 h.

≈360 K [6]. (The left inset is discussed later.) Three-dimensional long-range magnetic ordering is possible at lower temperatures, and is usually shown by the existence of a singularity (λ-type anomaly) in the specific heat vs. temperature at the magnetic transition temperature [35]. The variation of the magnetic specific heat of an antiferromagnet is closely similar to the behavior of the function d(χT)/dT, where χ is the zero-field susceptibility [36]. Fig. 3 shows a plot of d(χT)/dT in the temperature range between 100 and 400 K, exhibiting a sharp maximum at 262 K, which has previously been shown by neutron diffraction to correspond to the onset of long-range antiferromagnetic ordering [6]. In Fig. 2, a cooling history dependence of the susceptibility below ≈60 K is indicated by the splitting of the ZFC and FC data, whereas the two sets of data coincide above ≈60 K. A maximum appears at 46 K in the ZFC magnetization. The discrepancy between the ZFC and FC data has been attributed to a weak ferromagnetism due to spin canting [6]. The abrupt increase of magnetization below ≈60 K indicates the presence of a ferromagnetic component. These features of the starting o-$LiMnO_2$ are consistent with previous results for this compound [6].

Considering the folded triangular lattice in o-$LiMnO_2$, spin-glass behavior may be possible as a result of geometrical frustration and magnetic disorder. The possibility of spin-glass behavior coexisting with antiferromagnetic long-range ordering was not considered in Ref. [6]. We used the frequency dependence of the ac susceptibility and the time-dependence of magnetization to investigate spin-glass behavior [37]. The ac susceptibility was measured between 5 and 80 K at frequencies of 2, 20, 200, and 1000 Hz. The ac driving field was 1 Oe, and no external dc field was applied. Results in Fig. 4 show a maximum at 47 K, indicative of a magnetic phase transition below 47 K. The ac susceptibility is weakly frequency dependent below 47 K, increasing with decreasing frequency (see inset).

There is another maximum at 42 K in the ac susceptibility, consistent with the dc magnetization data (see left inset of

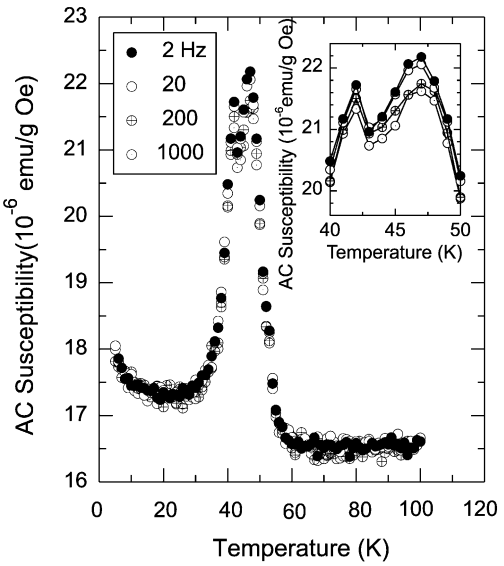

Fig. 4. Real part of the ac susceptibility of o-$LiMnO_2$ as a function of temperature between 5 and 100 K at the frequencies of 2, 20, 200, and 1000 Hz. The oxide sample was fired at $T = 950$ °C, $P_{O_2} = 10^{-6}$ atm for a total of 4 h.

Fig. 2). The second peak is attributed to the presence of XRD-undetected impurity phase having a different transition temperature. The appearance of the double-peak feature is sensitive to synthesis conditions that determine compositional homogeneity. Fig. 5 shows the dc magnetization in a magnetic field of 1000 Oe for the o-$LiMnO_2$ sample that was intermittently ground twice and fired at $T = 850$ °C, $P_{O_2} = 10^{-6}$ atm for a total of 5 h. Only one peak is seen at 41 K in the ZFC magnetization, indicating that the double-peak feature is not intrinsic to o-$LiMnO_2$. It is believed that a slight difference in the oxygen/metal stoichiometry of o-$LiMnO_2$ results in the different transition temperatures. Because the sample in Fig. 5 was ground twice, a more homogeneous reaction at the firing temperature is believed to

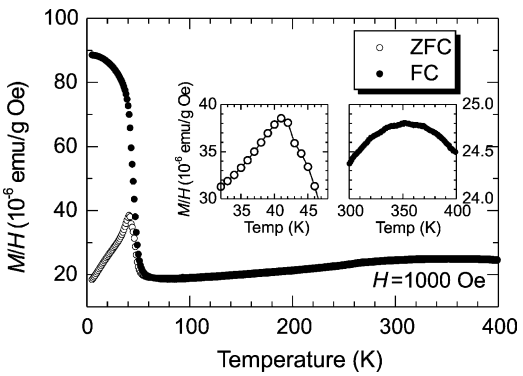

Fig. 5. Zero-field-cooled (ZFC) and field-cooled (FC) dc magnetization of o-$LiMnO_2$ as a function of temperature in a field of 1000 Oe. The oxide sample was fired at $T = 850$ °C, $P_{O_2} = 10^{-6}$ atm for a total of 5 h.

have occurred. The lattice parameters for this sample: $a = (2.8057 \pm 0.0005)$ Å, $b = (5.749 \pm 0.001)$ Å, and $c = (4.575 \pm 0.001)$ Å, are identical to those for the sample in Fig. 2 within the precision of the XRD measurement. The fact that firings at 850 and 950 °C followed by furnace-cooling result in nearly identical lattice parameters suggests that the two samples have nearly identical average Mn valences. For an oxide, it is well-known that higher temperatures are reducing and lower temperatures are oxidative at a fixed oxygen partial pressure [38]. However, the fast redox kinetics of $LiMnO_2$ make the two samples nearly indistinguishable after slow furnace-cooling. Quenching experiments have shown that the combined effects of cooling rate and firing atmosphere can have great impact on the phase of $LiMnO_2$ that is retained to room temperature [39].

To obtain the thermo-remanent magnetization (σ_{TRM}), we applied a field at 400 K and then cooled the sample in constant field to 5 K, at which point the field was switched off. Results for a field of 0.6 T showing slow decay of σ_{TRM} over ≈2 h are shown in Fig. 6. Decay of the magnetization for spin glasses can be modeled as a power law ($\sigma = \sigma_0 t^{-a}$), exponential ($\sigma = \sigma_0 \exp[-t]$), or stretched-exponential type ($\sigma = \sigma_0 \exp[-(t/\tau)^{1-n}]$) ($0 < n < 1$), where σ and σ_0 are the magnetization at time $t = 0$ and $t > 0$, respectively [37]. A plot of $\log\{-\mathrm{d}/\mathrm{d}t[\ln\sigma]\}$ vs. $\log\{t\}$, shown in the inset of Fig. 6, yields slope of $n = 1.1$, suggesting a power law dependence [40]. The isothermal remanent magnetization (σ_{IRM}) was obtained by cooling the sample in zero field from 400 to 5 K, at which point a field was applied for 5 min and then switched off. Fig. 7 compares the magnetic field dependences of σ_{TRM} and σ_{IRM}, both at $t = 1$ h, at 5 K. σ_{IRM} increases with increasing field and saturates above 3 T, while σ_{TRM} reaches a maximum at 0.8 T and then is nearly constant with field. These results suggest that o-$LiMnO_2$ exhibits spin-glass behavior in the temperature regime of long-range antiferromagnetic order, which could be explained by: (1) the spatial segregation of antiferromagnetic regions and spin-glass regions [21,25,28], or (2) spin canting [41–43], which also causes weak ferromagnetism [6]. The correct interpretation of this coexistent behavior is not presently known.

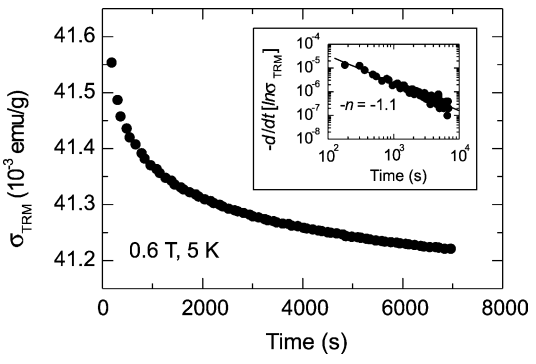

Fig. 6. Time dependence of σ_{TRM} of o-$LiMnO_2$ at 5 K after a field of 0.6 T is set to zero. The oxide sample was fired at $T = 950$ °C, $P_{O_2} = 10^{-6}$ atm for a total of 4 h.

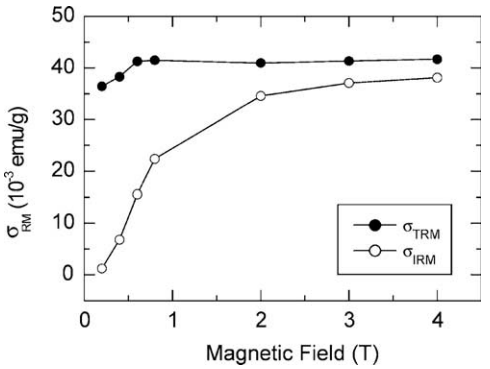

Fig. 7. Field dependence of σ_{IRM} and σ_{TRM} measured 1 h after setting the field to zero at 5 K. The oxide sample was fired at $T = 950$ °C, $P_{O_2} = 10^{-6}$ atm for a total of 4 h.

3.2. Delithiated, partially transformed sample

The delithiated sample was obtained by charging the $LiMnO_2$ composite cathode to 4.8 V as shown in Fig. 8. The final composition was determined from the delivered charge capacity (175 mAh/g) to be $Li_{0.39}MnO_2$, assuming that the capacity results from Li extraction only. Fig. 9 shows the XRD pattern of the composite cathode after charge. The broad and high background at low 2θ angles is due to the amorphous components of the composite electrode and the polymer tape used to protect the sample during XRD. The diffraction peaks of o-$LiMnO_2$ nearly disappear after the first charge to 4.8 V, indicating transformation to the spinel structure. The *hkl* indices indicated correspond to the space group $Fd\bar{3}m$. The lattice parameter for the charged sample has been calculated from the XRD data by a least-squares method to be: $a = 8.0 \pm 0.2$ Å. Note that the (400) and (440) peaks are much stronger than the (111) peak, indicating that rearrangement of the Mn ions to spinel is not complete. The (111) peak at $2\theta \approx 18°$ is normally

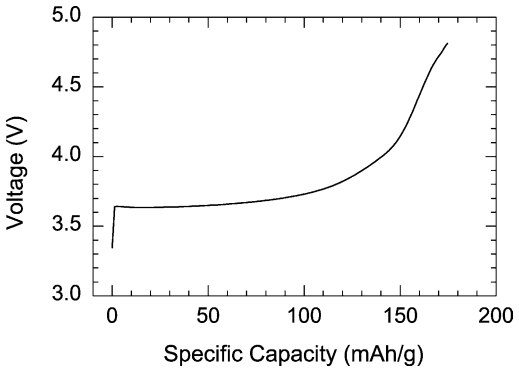

Fig. 8. Electrochemical preparation of $Li_{0.39}MnO_2$. o-$LiMnO_2$ was fired at $T = 950$ °C, $P_{O_2} = 10^{-6}$ atm for a total of 4 h, and was charged to 4.8 V against a Li metal anode at 24.6 mA/g rate.

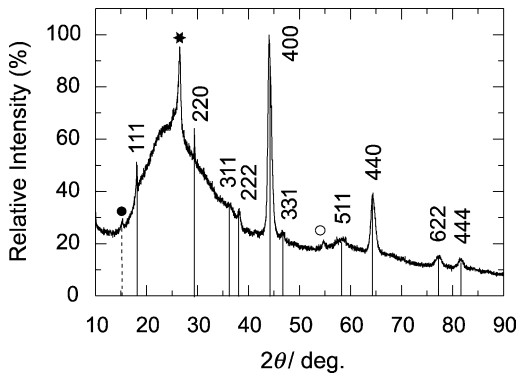

Fig. 9. X-ray diffraction pattern of $Li_{0.39}MnO_2$ electrodes after first charge. Miller indices *hkl* are indexed according to the $Fd\bar{3}m$ space group. • and ∗ represent *o*-$LiMnO_2$ and graphite, respectively.

the strongest peak in spinel of space group $Fd\bar{3}m$, and is absent for the rocksalt structure (space group $Fd\bar{3}m$). An antiphase nanodomain structure has been shown to form upon further cycling, giving Li/Mn ions distributed on either the 8*a*/16*d* or 8*b*/16*c* sites in space group $Fd\bar{3}m$ [4,5].

The existence of the (220) peak at $2\theta \approx 29.4°$ is a striking feature of the transformed spinel, indicating that a fraction of Mn ions are present on tetrahedral sites of the spinel structure [44,45]. The existence of this peak is consistent with our previous work using transmission electron microscopy (TEM) and electrochemical tests [3,4] showing that a fraction of the Mn ions occupy tetrahedral sites in transformed spinel. By electron diffraction in TEM, it was shown that new reflections not present in well-ordered spinel appear in transformed spinel due to tetrahedral site occupancy of the heavier Mn ions in place of Li. Electron diffraction is therefore sensitive to the location of Mn ions. Supporting this interpretation are the electrochemical tests in Ref. [3], which are sensitive to the insertion sites of Li ions. In that work the discharge capacity on the 3 V plateau relative to the capacity on the 4 V plateau was used to estimate the concentration of Li inserted onto octahedral vs. tetrahedral sites. The ratio of 3 V–4 V capacity was ~6 during the first discharge, showing preferential insertion of Li ions onto octahedral sites, which is reasonable if the tetrahedral sites are partially occupied by Mn ions.

Fig. 10 shows the dc magnetization of $Li_{0.39}MnO_2$ between 5 and 600 K in a magnetic field of 1000 Oe after ZFC and FC, respectively. The magnetization of the delithiated compound was calculated based on the weight of the oxide alone. From the weight percentage of starting $LiMnO_2$ in the composite cathode (69.8%) and the composition after charge ($Li_{0.39}MnO_2$), the weight percentage of the delithiated oxide in the composite cathode is calculated to be 68.8%. We initially performed measurements up to 400 K only. As discussed below, these results showed a Curie-Weiss fit yielding a Curie constant that could only be interpreted by assuming low-spin Mn ions on the tetrahedral sites. We then extended the measurements to

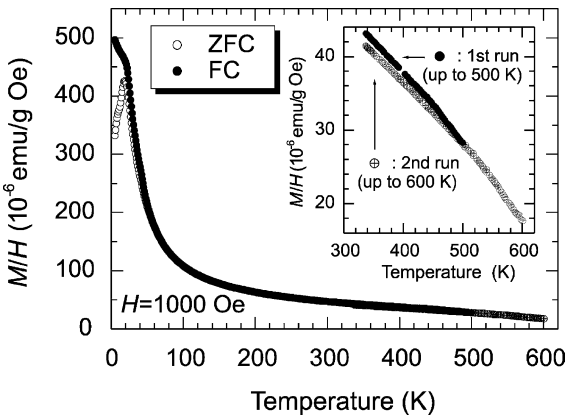

Fig. 10. Zero-field-cooled (ZFC) and field-cooled (FC) dc magnetization of $Li_{0.39}MnO_2$ as a function of temperature in a field of 1000 Oe. After measurements up to 500 K, the sample was cooled to 337 K and then reheated to 600 K.

higher temperature in two steps, being mindful of the possibility of irreversible changes occurring in the highly oxidized, partially ordered sample upon heating. The inset in Fig. 10 shows results for two heating runs, the first during heating from 337 to 500 K, and the second for a subsequent measurement during heating from 337 to 600 K. The results show that irreversible changes do occur upon heating to these higher temperatures. After heating to 500 K, there is a small reduction (~4%) in the magnetization measured at 337 K, compared to the initial measurements. After the second run heating to 600 K, a further reduction in the magnetization of ~17% relative to the initial value is observed. These irreversible changes, attributed to rearrangement of structure and/or changes in composition upon heating of the highly oxidized sample, are seen very clearly in the inverse susceptibility plots in Fig. 11. Based on this clear evidence for instability of the sample above

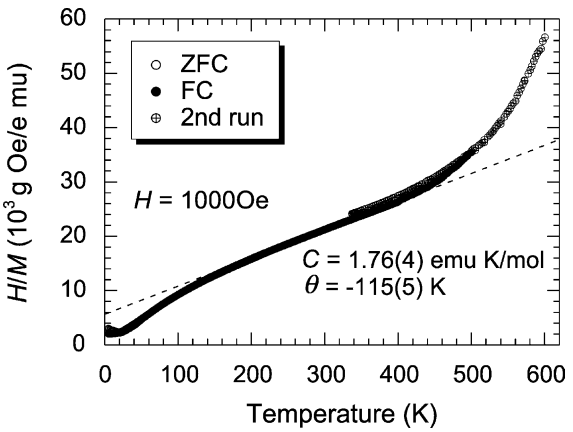

Fig. 11. Inverse zero-field-cooled (ZFC) and field-cooled (FC) dc magnetization of $Li_{0.39}MnO_2$ as a function of temperature in a field of 1000 Oe. After measurements up to 500 K, the sample was cooled to 337 K and then reheated to 600 K.

400 K, we focus on the temperature region below 400 K in analyzing the data.

The magnetic behavior of the transformed spinel is clearly distinguishable from that of the starting *o*-$LiMnO_2$. The broad maximum centered at $\approx$360 K has disappeared (compare Figs. 5 and 10), indicating that the two-dimensional short-range spin correlation does not occur upon cooling of the transformed spinel. This can be explained by the destruction of the folded triangular lattice of *o*-$LiMnO_2$ that accompanies the partial, incomplete transformation to spinel ordering during delithiation. The inverse susceptibility is plotted in Fig. 11, including a Curie-Weiss law fit to the data obtained between 200 and 400 K. The square of correlation coefficient (R^2) of the fitting was 0.9999. This excellent fit gave Weiss and Curie constants of $\Theta = -(115 \pm 5)$ K and $C = (1.76 \pm 0.04)$ cm^3 K/mol. The negative Weiss constant indicates that antiferromagnetic interactions predominate in the transformed spinel, as is the case for $Li_{0.07}Mn_2O_4$ ($\Theta = -74$ K) and $Li_{0.98}Mn_2O_4$ ($\Theta = -250$ K) prepared by electrochemical cycling of $LiMn_2O_4$ [25]. From the Curie constant, the effective moment is determined to be $\mu_{eff} = (3.76 \pm 0.01)\ \mu_B$, where μ_B is the Bohr magneton, 0.927×10^{-20} erg/Oe. As the preferred migration path for Mn ions during the transformation is believed to be via tetrahedral sites [8,44], it is likely that Li and Mn ions occupy both octahedral and tetrahedral sites in a disordered distribution [5]. For $Li_{0.39}MnO_2$, 39 and 61% of Mn ions have the valence of 3 + and 4 +, respectively. Recent ab initio calculations by Reed et al. [46] suggested occupancy of the tetrahedral sites by Mn^{2+} through a charge disportionation reaction

$$2Mn^{3+}_{oct} \rightarrow Mn^{2+}_{tet} + Mn^{4+}_{oct} \quad (1)$$

We consider the following possible site occupancies of Li and Mn ions in $Li_{0.39}MnO_2$.

$$(Li_{0.39-x}Mn^{2+}_{y})_{tet}[Li_xMn^{3+}_{0.39-2y}Mn^{4+}_{0.61+y}]_{oct}O_2 \quad (2)$$

$$(Li_{0.39-x}Mn^{3+}_{y})_{tet}[Li_xMn^{3+}_{0.39-y}Mn^{4+}_{0.61}]_{oct}O_2 \quad (3)$$

$$(Li_{0.39-x}Mn^{4+}_{y})_{tet}[Li_xMn^{3+}_{0.39}Mn^{4+}_{0.61-y}]_{oct}O_2 \quad (4)$$

Here, the octahedral Mn^{3+} and Mn^{4+} ions have the electronic configurations of $t^3_{2g}e^1_g(J = 2)$ and $t^3_{2g}e^0_g(J = 3/2)$, respectively. On tetrahedral sites, low-spin Mn^{2+} and Mn^{4+} have the electronic configurations of $e^4t^1_2(J = 1/2)$ and $e^3t^0_2(J = 1/2)$, respectively, while low-spin Mn^{3+} is in the $e^4t^0_2(J = 0)$ configuration. The theoretical Curie constants for the Mn ions with $J = 1/2, 3/2$, and 2 are 0.37, 1.87, and 3.00 cm^3 K/mol, respectively. The overall theoretical Curie constants are $[0.37y + 3(0.39 - 2y) + 1.87{\cdot}(0.61 + y)]$, $[3(0.39 - y) + 1.87{\cdot}0.61]$, and $[0.37y + 3{\cdot}0.39 + 1.87{\cdot}(0.61 - y)]$ cm^3 K/mol, respectively, for the site occupancies of Eqs. (2)–(4). By equating the overall theoretical values with the experimental Curie constant (1.76 cm^3 K/mol), we can determine that the fraction of tetrahedral Mn ion has a surprisingly high value of $y = 0.15$ (Mn^{2+}, Eq. (2)), $y = 0.18$ (Mn^{3+}, Eq. (3)), and $y = 0.37$ (Mn^{4+}, Eq. (4)) for the possible site occupancies shown above. As the Li ions are nonmagnetic, x cannot be determined from the Curie constant. The Mn valence on the tetrahedral sites cannot be determined based solely on the present results given that the experimental Curie constant can be fit to each of the above ion distributions with y as a variable.

While the Curie–Weiss fit is obtained over a limited temperature regime, we note that in Fig. 11 the inverse susceptibility shows an upward curvature above 400 K, and therefore extending the fit to >400 K would result in a lower Curie constant and, in turn, even higher fractions of tetrahedral Mn ions. However, due to the irreversible changes to the sample at higher temperatures, we believe that the data below 400 K is most representative of the electrochemically transformed sample.

Note that the proposed site occupancies have the surprising feature of low-spin Mn ions on the tetrahedral sites. The experimental value of the Curie constant cannot be obtained when assuming tetrahedral site occupancy of high-spin Mn^{2+} ($e^2t^3_2$), Mn^{3+} ($e^2t^2_2$), or Mn^{4+} ($e^2t^1_2$). The tetrahedral low-spin state might appear improbable, since the tetrahedral geometry results in smaller crystal field splitting than the octahedral geometry for a given ligand. High-spin configurations are generally observed in the tetrahedral geometry [47]. However, the existence of tetrahedral low-spin ions has been suggested in sulfides [48,49] and spinel oxides [50–52]. The unusual spin state that we deduce from these experimental results may be due to incomplete spinel ordering and the high level of local mechanical stress that is known to result from electrochemical delithiation [4,5]. Clearly, further studies would be beneficial to confirm the unusual spin state and site occupancy of Mn ions in these spinels.

To our knowledge, these are the first quantitative measurements of the distribution of Mn ions between tetrahedral and octahedral sites during the electrochemically-induced spinel transformation in $LiMnO_2$ compounds. The results support previous work from our group using TEM and electrochemical tests [3–4] showing that a fraction of the Mn ions occupy tetrahedral sites in transformed spinel. The present magnetization results are, like the TEM results, sensitive to the distribution of Mn rather than that of Li. They are completely consistent with both of these prior measurements in showing that there are tetrahedral Mn ions after the first charge, but provide a more quantitative measure of the distribution than either. The site distribution of Mn undoubtedly depends on electrochemical test conditions such as current density and temperature, and it is generally believed that continued cycling causes the Mn ions to be increasingly ordered on the spinel octahedral sites. This study shows that magnetic characterization can be used to follow the evolution of this cation ordering upon electrochemical cycling.

It is of interest to compare the Curie constant for the transformed spinel $Li_{0.39}MnO_2$ with the values for

highly-ordered, conventional spinels $Li_xMn_2O_4$. Previously, Greedan and coworkers reported that the Curie constants for λ-MnO_2 ($x \sim 0.2$) and $LiMn_2O_4$ are 1.97 and 2.43 cm^3 K/mol, respectively, per mole of Mn ions [20,22]. It is notable that the Curie constant for the transformed spinel (1.76 cm^3 K/mol for $Li_{0.39}MnO_2$) is lower than those in these conventional spinels. We attribute this result to the presence of low spin Mn ions on the tetrahedral sites, for which the Curie constant is 0.37 cm^3 K/mol (in the case of Mn^{2+} and Mn^{4+}) or even zero (in the case of Mn^{3+}). Octahedral Mn^{4+} and Mn^{3+} ions have higher Curie constants of 1.87 and 3.00 cm^3 K/mol, respectively.

The splitting of the ZFC and FC curves in Fig. 10 shows that a cooling history dependence sets in below ≈40 K. Fig. 12 shows the temperature dependence of the ac susceptibility measured between 5 and 100 K at frequencies of 20, 200, and 1000 Hz (1 Oe ac driving field, no external dc field). The sharp peak at 21 K in Fig. 12 is coincident with the peak in the ZFC curve in Fig. 10, and is indicative of a magnetic phase transition below 21 K. A frequency dependence of the ac susceptibility is also observed below ≈21 K. The results in Figs. 10 and 12 indicate that spin-glass behavior occurs in the transformed spinel $Li_{0.39}MnO_2$ with a freezing temperature of $T_f = 21$ K. The time-dependent remanent magnetization results for the delithiated sample in Figs. 13 and 14, measured in the same manner as for the starting *o*-$LiMnO_2$ in Figs. 6 and 7, are consistent with this interpretation of spin-glass behavior. The inset of Fig. 13 also suggests a power-law dependence for decay of magnetization. As in $Li_xMn_2O_4$ spinels [13,20–23,25,26], the spin-glass behavior appears to coexist with antiferromagnetic ordering in $Li_{0.39}MnO_2$.

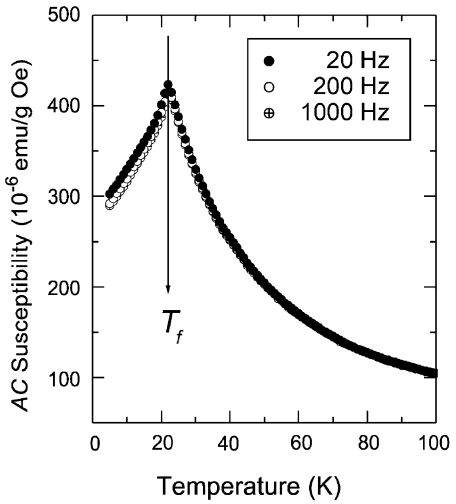

Fig. 12. Real part of the ac susceptibility of $Li_{0.39}MnO_2$ as a function of temperature between 5 and 100 K at the frequencies of 20, 200, and 1000 Hz. T_f indicates the freezing temperature.

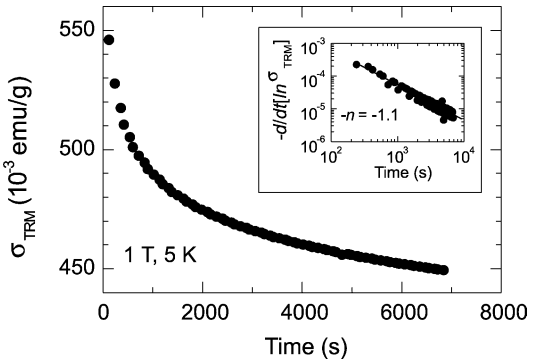

Fig. 13. Time dependence of σ_{TRM} of $Li_{0.39}MnO_2$ at 5 K after a field of 1 T is set to zero.

We can further compare the results of this study with previous studies [21,25] of spin-glass behavior in this class of manganates, keeping in mind that frustration and randomness are the necessary conditions for spin-glass behavior [37,53]. The freezing temperature of $Li_{0.39}MnO_2$, lies between those of delithiated spinel $Li_{0.07}Mn_2O_4$ ($T_f = 16$ K) and nearly stoichiometric $Li_{0.98}Mn_2O_4$ ($T_f = 25$ K). This is qualitatively consistent with the observed trend for conventional spinels that T_f decreases with increasing Mn valence [13,25]. It has been suggested that spin freezes at lower temperatures as the strength of antiferromagnetic interactions decreases [25]. As the Mn valence increases, the fraction of ferromagnetic coupling (Mn^{4+}–O^{2-}–Mn^{4+}) increases, decreasing the geometrical frustration of the tetrahedral anitiferromagnetic lattice in the $[Mn_2]O_4$ spinel framework. Since the Mn sublattice of the present sample is partially ordered while the others are completely ordered in the spinel framework, some differences are to be expected. An empirical measure of frustration in spin glasses is $f = |\Theta|/T_f$ [53]. (The measure of frustration $|\Theta|/T_c$, where T_c represents a cooperative-ordering transition temperature, is generally applicable to

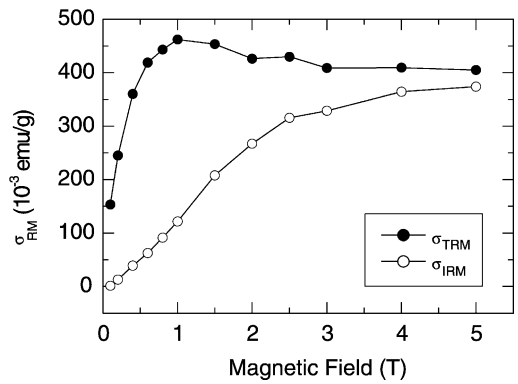

Fig. 14. Field dependence of σ_{IRM} and σ_{TRM} of $Li_{0.39}MnO_2$ measured 1 h after setting the field to zero at 5 K.

antiferromagnetics and spin glasses). For $Li_{0.39}MnO_2$, f is calculated to be ≈ 5 from the present data. This is a lower degree of frustration closer to that of λ-MnO_2 ($f = 5-6$) than that of $LiMn_2O_4$ spinel ($f = 10-14$, calculated from literature data [11–15,17–18,20–22,25]). In highly-ordered $LiMn_2O_4$, the antiferromagnetic tetrahedral network of Mn ions on 16*d* sites gives rise to geometric frustration [22]. In $Li_{0.39}MnO_2$, this tetrahedral network is incomplete and it is reasonable to expect a lower degree of geometric frustration. As spinel ordering improves with further cycling of the *o*-$LiMnO_2$ [3], we would expect the degree of geometric frustration in the transformed spinel to systematically increase. Similar behavior is expected to occur in the transformed spinel obtained by delithiation of monoclinic phase $LiMnO_2$, which also irreversibly transforms to the spinel structure during electrochemical cycling [5,54–56].

4. Conclusions

Bulk magnetic characterization was performed on orthorhombic $LiMnO_2$ and delithiated $Li_{0.39}MnO_2$ that has partially transformed to the spinel structure. In $LiMnO_2$, evidence of short-range magnetic correlations below ≈ 360 K and long-range antiferromagnetic ordering below 262 K were observed, consistent with previous reports [6]. However, the magnetic behavior of $LiMnO_2$ is further complicated by spin-glass behavior occurring within the temperature regime of long-range antiferromagnetic ordering. In $Li_{0.39}MnO_2$, it is found that the short-range and long-range magnetic orderings are lost, while spin-glass behavior remains. The fraction of Mn ions occupying tetrahedral sites in the partially transformed spinel has been quantitatively determined for the first time, using magnetic susceptibility data in the paramagnetic temperature regime. Furthermore, an unusual site occupancy of low-spin Mn ions on tetrahedral sites is proposed. A comparison of the spin-glass behavior in $Li_{0.39}MnO_2$ with conventional spinel $LiMn_2O_4$ suggests that $Li_{0.39}MnO_2$ has a lower degree of frustration, which is attributed to incomplete spinel ordering, providing less geometrical frustration than in the ordered spinel structure. Magnetic characterization is shown to be an effective tool for probing the spinel transformation of orthorhombic and monoclinic $LiMnO_2$.

Acknowledgements

This study was supported by NSF Grant no. 9400334-DMR, and used instrumentation in the Shared Experimental Facilities at MIT. Partial support for B.H. was provided by Intronics and the Office of Naval Research (N00014-99-1-0565). MIT contributed matching funds from the MacVicar Foundation in the form of a faculty fellowship for DRS.

References

[1] T. Ohzuku, A. Ueda, T. Harai, Chem. Express 7 (1992) 193.
[2] M.M. Thackeray, Prog. Solid State Chem. 25 (1997) 1.
[3] Y.-I. Jang, B. Huang, H. Wang, D.R. Sadoway, Y.-M. Chiang, J. Electrochem. Soc. 146 (1999) 3217.
[4] H. Wang, Y.-I. Jang, Y.-M. Chiang, Electrochem. Solid-State Lett. 2 (1999) 490.
[5] Y.-M. Chiang, H. Wang, Y.-I. Jang, Chem. Mater. 13 (2001) 53.
[6] J.E. Greedan, N.P. Raju, I.J. Davidson, J. Solid State Chem. 128 (1997) 209.
[7] J.N. Reimers, E.W. Fuller, E. Rossen, J.R. Dahn, J. Electrochem. Soc. 140 (1993) 3396.
[8] R.J. Gummow, D.C. Liles, M.M. Thackeray, Mater. Res. Bull. 28 (1993) 1249.
[9] R.J. Gummow, M.M. Thackeray, J. Electrochem. Soc. 141 (1994) 1178.
[10] I.M. Kötschau, J.R. Dahn, J. Electrochem. Soc. 145 (1998) 2672.
[11] G. Blasse, J. Phys. Chem. Solids 27 (1966) 383.
[12] L. Schütte, G. Cosmann, B. Reuter, J. Solid State Chem. 27 (1979) 227.
[13] P. Endres, B. Fuchs, S. Kemmler-Sack, K. Brandt, G. Faust-Becker, H.-W. Praas, Solid State Ionics 89 (1996) 221.
[14] N. Kumagai, T. Fujiwara, K. Tanno, T. Horiba, J. Electrochem. Soc. 143 (1996) 1007.
[15] C. Masquelier, M. Tabuchi, K. Ado, R. Kanno, Y. Kobayashi, Y. Maki, O. Nakamura, J.B. Goodenough, J. Solid State Chem. 123 (1996) 255.
[16] M. Tabuchi, C. Masquelier, H. Kobayashi, R. Kanno, Y. Kobayashi, T. Akai, Y. Maki, H. Kageyama, O. Nakamura, J. Power Sources 68 (1997) 623.
[17] J. Sugiyama, T. Hioki, S. Noda, M. Kontani, J. Phys. Soc. Jpn. 66 (1997) 1187.
[18] J. Sugiyama, T. Hioki, S. Noda, M. Kontani, Mater. Sci. Engng B54 (1998) 73.
[19] C.B. Azzoni, M.C. Mozzati, A. Paleari, V. Massarotti, D. Capsoni, M. Bini, Z. Naturforsch 53a (1998) 693.
[20] J.E. Greedan, N.P. Raju, A.S. Wills, C. Morin, S.M. Shaw, J.N. Reimers, Chem. Mater. 10 (1998) 3058.
[21] Y.-I. Jang, F.C. Chou, Y.-M. Chiang, Appl. Phys. Lett. 74 (1999) 2504.
[22] A.S. Wills, N.P. Raju, J.E. Greedan, Chem. Mater. 11 (1999) 1510.
[23] A.S. Wills, N.P. Raju, C. Morin, J.E. Greedan, Chem. Mater. 11 (1999) 1936.
[24] V. Massarotti, D. Capsoni, M. Bini, G. Chiodelli, C.B. Azzoni, M.C. Mozzati, A. Paleari, J. Solid, State Chem. 147 (1999) 509.
[25] Y.-I. Jang, B. Huang, F.C. Chou, D.R. Sadoway, Y.-M. Chiang, J. Appl. Phys. 87 (2002) 7382.
[26] I. Tomeno, Y. Kasuya, Y. Tsunoda, Phys. Rev. B64 (2001) 094422.
[27] Y. Oohara, J. Sugiyama, M. Kontani, J. Phys. Soc. Jpn. 68 (1999) 242.
[28] J.E. Greedan, C.R. Wiebe, A.S. Wills, J.R. Stewart, Phys. Rev. B65 (2002) 184424.
[29] Y.-M. Chiang, Y.-I. Jang, H. Wang, B. Huang, D.R. Sadoway, P. Ye, J. Electrochem. Soc. 145 (1998) 887.

[30] Y.-I. Jang, H. Wang, Y.-M. Chiang, J. Mater. Chem. 8 (1998) 2761.
[31] Y.-I. Jang, Y.-M. Chiang, Solid State Ionics 130 (2000) 53.
[32] B. Huang, Y.-I. Jang, Y.-M. Chiang, D.R. Sadoway, J. Appl. Electrochem. 28 (1998) 1365.
[33] R. Hoppe, G. Brachtel, M. Jansen, Z. Anorg. Allg. Chem. 417 (1975) 1.
[34] L. Croguennec, P. Deniard, R. Brec, A. Lecerf, J. Mater. Chem. 7 (1997) 511.
[35] S. Chikazumi, S.H. Charap, Physics of Magnetism, Wiley, New York, 1964.
[36] M.E. Fisher, Philos. Mag. 7 (1962) 1731.
[37] K. Binder, A.P. Young, Rev. Mod. Phys. 58 (1986) 801.
[38] D.R. Gaskell, Introduction to Metallurgical Thermodynamics, second ed., Hemisphere, Washington, 1981.
[39] Y.-I. Jang, W.D. Moorehead, Y.-M. Chiang, Solid State Ionics 149 (2002) 201.
[40] R.V. Chamberlin, J. Appl. Phys. 57 (1985) 3377.
[41] Y.-I. Jang, F.C. Chou, Y.-M. Chiang, J. Phys. Chem. Solids 60 (1999) 1763.
[42] J.E. Greedan, N.P. Raju, A. Maignan, Ch. Simon, J.E. Pedersen, A.M. Niraimathi, E. Gmelin, M.A. Subramanian, Phys. Rev. B54 (1996) 7189.
[43] M.A. Girtu, C.M. Wynn, W. Fujita, K. Awaga, A.J. Epstein, Phys. Rev. B57 (1998) R11 058.
[44] J.M. Tarascon, E. Wang, F.K. Shokoohi, W.R. McKinnon, S. Colson, J. Electrochem. Soc. 138 (1991) 2859.
[45] H. Wang, Y.-I. Jang, B. Huang, D.R. Sadoway, Y.-M. Chiang, J. Electrochem. Soc. 146 (1999) 473.
[46] J. Reed, G. Ceder, A. Van der Ven, Electrochem. Solid State Lett. 4 (2001) A78.
[47] F.A. Cotton, G. Wilkinson, C.A. Murillo, M. Bochmann, Advanced Inorganic Chemistry, sixth ed., Wiley, New York, 1999.
[48] W. Bronger, P. Müller, J. Less-Comm, Metals 70 (1980) 253.
[49] W. Bronger, A. Kyas, P. Müller, J. Solid State Chem. 70 (1987) 262.
[50] P.D. Battle, A.K. Cheetham, J.B. Goodenough, Mater. Res. Bull. 14 (1979) 1013.
[51] A.B. Devale, D.K. Kulkarni, J. Phys. C: Solid State Phys. 15 (1982) 899.
[52] V.P. Pashchenko, A.V. Kopaev, G.T. Brovkina, A.K. Prokopenko, I.F. Klochai, Inorg. Mater. 21 (1985) 1544.
[53] A.P. Ramirez, Annu. Rev. Mater. Sci. 24 (1994) 453.
[54] A.R. Armstrong, P.G. Bruce, Nature 381 (1996) 499.
[55] F. Capitaine, P. Gravereau, C. Delmas, Solid State Ionics 89 (1996) 197.
[56] Y.-I. Jang, B. Huang, Y.-M. Chiang, D.R. Sadoway, Electrochem. Solid-State Lett. 1 (1998) 13.